

RESEARCH ARTICLE

Non-Selective Evolution of Growing Populations

Karl Wienand¹ , Matthias Lechner¹ , Felix Becker² , Heinrich Jung², Erwin Frey¹ *

1 Arnold-Sommerfeld-Center for Theoretical Physics and Center for NanoScience, Physics Department, Ludwig-Maximilians-Universität, Munich, Germany, **2** Department of Biology 1, Microbiology, Ludwig-Maximilians-Universität, Martinsried, Germany

 These authors contributed equally to this work.

* frey@lmu.de



 OPEN ACCESS

Citation: Wienand K, Lechner M, Becker F, Jung H, Frey E (2015) Non-Selective Evolution of Growing Populations. PLoS ONE 10(8): e0134300. doi:10.1371/journal.pone.0134300

Editor: Matjaz Perc, University of Maribor, SLOVENIA

Received: May 8, 2015

Accepted: July 7, 2015

Published: August 14, 2015

Copyright: © 2015 Wienand et al. This is an open access article distributed under the terms of the [Creative Commons Attribution License](https://creativecommons.org/licenses/by/4.0/), which permits unrestricted use, distribution, and reproduction in any medium, provided the original author and source are credited.

Data Availability Statement: All relevant data are within the paper and its Supporting Information files.

Funding: EF was funded by the Deutsche Forschungsgemeinschaft, Priority Programme 1617 "Phenotypic heterogeneity and sociobiology of bacterial populations", grant FR 850/11-1 and the German Excellence Initiative via the programme "Nanosystems Initiative Munich" (NIM). HJ was funded by the Deutsche Forschungsgemeinschaft, Priority Programme 1617 "Phenotypic heterogeneity and sociobiology of bacterial populations", grant JU 333/5-1 (<http://www.spp1617.org/>). KW was supported by the Elitenetzwerk Bayern. The funders had no role in study design, data collection and

Abstract

Non-selective effects, like genetic drift, are an important factor in modern conceptions of evolution, and have been extensively studied for constant population sizes (Kimura, 1955; Otto and Whitlock, 1997). Here, we consider non-selective evolution in the case of growing populations that are of small size and have varying trait compositions (e.g. after a population bottleneck). We find that, in these conditions, populations never fixate to a trait, but tend to a random limit composition, and that the distribution of compositions "freezes" to a steady state. This final state is crucially influenced by the initial conditions. We obtain these findings from a combined theoretical and experimental approach, using multiple mixed subpopulations of two *Pseudomonas putida* strains in non-selective growth conditions (Matthijs et al, 2009) as model system. The experimental results for the population dynamics match the theoretical predictions based on the Pólya urn model (Eggenberger and Pólya, 1923) for all analyzed parameter regimes. In summary, we show that exponential growth stops genetic drift. This result contrasts with previous theoretical analyses of non-selective evolution (e.g. genetic drift), which investigated how traits spread and eventually take over populations (fixate) (Kimura, 1955; Otto and Whitlock, 1997). Moreover, our work highlights how deeply growth influences non-selective evolution, and how it plays a key role in maintaining genetic variability. Consequently, it is of particular importance in life-cycles models (Melbinger et al, 2010; Cremer et al, 2011; Cremer et al, 2012) of periodically shrinking and expanding populations.

Introduction

Stochastic effects play an important role in population dynamics [8–11], particularly when competition between individuals is non-selective. Most previous theoretical analyses have studied how a non-selectively evolving trait can spread and eventually replace all other variants (fixate) under conditions in which the population size remains constant [2, 12, 13]. However, both natural and laboratory populations frequently experience exponential growth. Here we show that genetic diversity in growing populations is maintained despite demographic noise,

analysis, decision to publish, or preparation of the manuscript.

Competing Interests: The authors have declared that no competing interests exist.

and reaches a stationary but random limit. We used a well-controlled model system in which well-mixed co-cultures of a wild-type *Pseudomonas putida* strain and an isogenic mutant were grown under non-selective conditions. Multiple subpopulations were generated, each containing a random number of individuals of each strain. Depending on the average initial population size and the strain ratio, we observed distinct stationary probability distributions for their genetic composition. Moreover, we showed that the dynamics of growing populations can be mapped to Pólya urn models [4], permitting the observed maintenance of genetic diversity to be understood as the random limit property of a fair game between individual strains. Generalizing the Pólya urn model to include the effects of random initial sampling and exponential growth allowed us to predict the evolution of the composition distribution. Using numerical and analytical methods we found that the distribution broadens at first but quickly “freezes” to a stationary distribution, which agrees with the experimental findings. Our results provide new insights into the role of demographic noise in growing populations.

Results and Discussion

Evolutionary dynamics is driven by the complex interplay between selective and non-selective (or neutral) effects. The paradigm of non-selective evolution originates from the seminal work of Kimura [1], in which he solved the Wright-Fisher model, thus showing that non-selective effects—and specifically genetic drift—can have a determinant role in evolution. His results sparked an ongoing debate about the nature and potency of randomness as a fundamental evolutionary force [13–15]. For very small populations genetic drift is generally considered an important factor [13], as the theory successfully predicts the outcomes of neutral evolution experiments [9, 16].

In most theoretical analyses, constant (or effectively constant) population sizes are assumed, and the role of population growth is neglected. Bacterial populations, however, often undergo rapid growth—especially when they are small. For example, as few as 10 individuals of some highly virulent pathogens (e.g. enterohemorrhagic *Escherichia coli* or *Shigella dysenteriae*) suffice to initiate a deadly infection in a human host [17, 18]. Another case of small, growing populations are water-borne bacteria that feed on phytoplankton products. Due to nutrient limitation in open water, these bacteria typically live in small populations in close proximity to the planktonic organism [19]. During spring blooms, the phytoplankton releases more organic material, boosting the bacterial growth rate [19–21]. In nature, such small populations often form by adventitious dispersal from a larger reservoir population [22]. A typical example is the spreading of pathogens from host to host. This random “sampling” from a reservoir yields small populations whose genetic compositions differ from that of the reservoir (a phenomenon known as the *founder effect* [23]). Recent studies also showed that the combination of population growth and stochastic fluctuations can have a major impact on the evolution [5–7, 24] and genetics [25] of small populations.

To probe how population growth shapes genetic diversity, we used a well-characterized microbial model system, namely the soil bacterium *Pseudomonas putida* KT2440 [3, 29, 27]. The wild-type strain KT2440 produces pyoverdine, an iron-scavenging molecule that supports growth when iron becomes scarce in the environment. Here we consider co-cultures of two genetically distinct strains: the wild-type, pyoverdine-producing strain KT2440 (strain A) and the mutant non-producer strain 3E2 (strain B). We set up conditions of non-selective competition between these strains by using an iron-replete medium (casamino acids, supplemented with 200 μM FeCl_3). In this medium, production of pyoverdine is effectively repressed [27], such that both strains have the same growth rate and neither has an advantage (see S2 Table). Producer (KT2440 wild type) and non-producer (3E2) strains were first mixed and diluted to

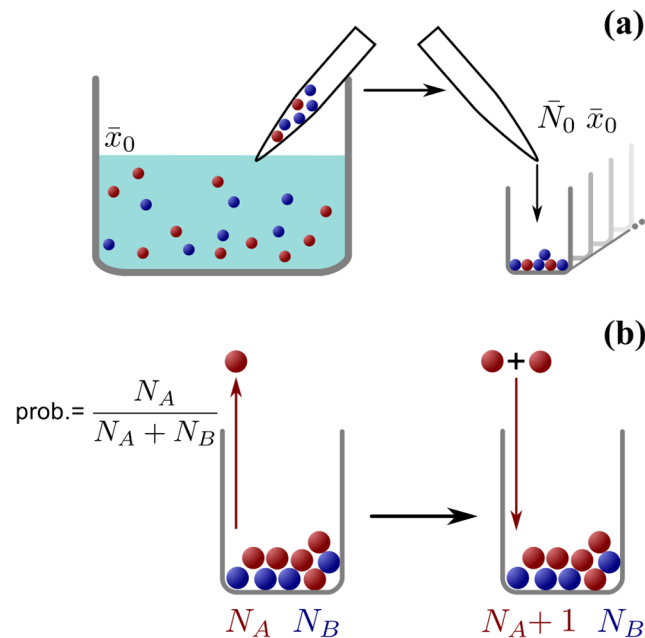


Fig 1. Schematic depiction of urn sampling and growth. (a) Schematic illustration of the random initial conditions. An infinite reservoir contains a diluted mixture of bacteria, a fraction \bar{x}_0 of which are of strain A. We draw small volumes of liquid from the reservoir containing small, random numbers of individuals, which conform to a Poisson distribution with mean (determined by the dilution of the reservoir population). A certain fraction of this initial population is of strain A. The mean value of this fraction is equal to \bar{x}_0 . We use these individuals to initiate populations in the wells of a microtiter plate, so that each population starts with a random size \bar{N}_0 and a random fraction of A-individuals \bar{x}_0 . (b) Illustration of the Pólya urn model. If a bacterial population is represented as an urn, each individual as a marble and each bacterial strain as a color, this urn model captures the essentials of bacterial reproduction in our populations. At each iteration, a marble is drawn at random and returned to the urn, together with another one of the same color. The probability of extracting a marble of either color is determined solely by its relative abundance, making the process non-selective (since no strain has inherent advantages, see S2 Table). The rate of growth in population size can be rendered exponential (see S2 Fig) by letting the waiting time between successive iterations be exponentially distributed (also known as Poissonization).

doi:10.1371/journal.pone.0134300.g001

yield Poisson dilution conditions. Then we initiated a large number of subpopulations from this reservoir by pipetting aliquots of the cell suspension into the wells of a 96-well plate, thereby generating a large ensemble of subpopulations with a random distribution of initial cell number N_0 and producer fraction x_0 (Fig 1). Use of shaken liquid cultures ensured homogeneous well-mixed conditions for all cells in the same well (access to nutrients, oxygen, etc.), and exponential growth was observed in all cases (see S2 Fig).

This experimental setting is well described within the mathematical framework of a *Pólya urn model*. Consider each bacterium in the population as a marble in an urn, and its genotype as the color of the marble (e.g. red for strain A, and blue for strain B). Population growth results from single reproduction events in which an individual randomly divides. This is mathematically equivalent to a stochastic event in which a marble is chosen at random from the urn and put back, together with another one of the same color. This random process, introduced by Eggenberger and Pólya [4], exhibits several important properties [28–31]. It is *self-reinforcing*: each time a marble is extracted, another one of the same color is added, increasing the likelihood of extracting a marble of that color again. In the context of bacterial populations, this means that every birth event for one strain makes it more likely that further birth events of that same strain will occur in the future. Note, however, that *fixation*, i.e., complete loss of one type

of marble from the population, cannot occur, simply because in the Pólya urn model marbles are neither removed nor do they change their color. This fully reflects the experimental conditions: During exponential growth, rates of cell death are negligible, and within the observation time mutations will be extremely rare, given the population sizes considered. The bacteria in each well reproduce randomly at a per-capita (average) rate μ . To translate this to the urn model, drawing of a marble is assumed to be a stochastic Poisson process, with a “per-marble” rate μ (a procedure known as *Poissonization* or *embedding* [32, 33]). Mathematically, the growth process is then described by a Master Equation: The time evolution for the probability $P(N_A, t)$ of finding N_A individuals of strain A at time t reads

$$\frac{d}{dt}P(N_A; t) = (N_A - 1)P(N_A - 1; t) - N_A P(N_A; t), \quad (1)$$

where we have set the growth rate to $\mu = 1$ in order to fix the time scale (for an introduction to the mathematical concepts see, e.g., [34]); the corresponding Master equation for individuals of strain B is of identical form. To study the composition of the populations, we use the more convenient quantities $N = N_A + N_B$ (total size) and $x = N_A/N$ (fraction of individuals of strain A).

To start the experiment, we inoculated the wells of 96-well-plates by drawing small volumes of diluted liquid bacterial culture from a large reservoir (Fig 1(a)). Each volume contains a random number of bacteria whose mean value is controlled by the dilution of the reservoir. The fraction of bacteria of strain A (wild type) in that volume is also random, with its mean value \bar{x}_0 given by the fraction of strain A in the reservoir. In the mathematical formulation, this setup corresponds to stochastic initial conditions for the Pólya urn model: the initial population size N_0 for each well is given by a Poisson distribution with mean \bar{N}_0 , and each individual is assigned to strain A or B with probability \bar{x}_0 and $1 - \bar{x}_0$, respectively. This procedure is also equivalent to treating the initial numbers of A - and B -individuals as independent, Poisson-distributed random variables with mean values $\bar{N}_0 \bar{x}_0$ and $\bar{N}_0 (1 - \bar{x}_0)$, respectively [6].

Fig 2 shows a time series of the histogram for the composition x of all subpopulations considered, as obtained from a stochastic simulation of the Master Eq (1) for a given random initial condition (with $\bar{N}_0 = 10$ and $\bar{x}_0 = 0.33$). Surprisingly, the distribution first broadens, but then quickly “freezes” to a steady state (see S1 Video). This is genuinely different from Kimura’s result for populations with constant size [1] (or similar results with effectively constant size [2]) where the balance between stochastic birth and death events leads to genetic drift, and thereby eventually to the extinction of one of the two strains. In contrast, for a growing population, death events are negligible, and therefore there is no fixation of the population during growth. Instead, fixation arises as a direct consequence of the initial sampling process, as can be seen from the heights of the black bins in the histogram (at $x = 0$ and $x = 1$), which remain constant over time (Fig 2). During growth, the composition of each subpopulation, instead of drifting to fixation at either $x = 0$ or $x = 1$, reaches a stationary limit value x^* , where it remains thereafter [35]. This limit value is random: starting several subpopulations (urns) from the exact same initial composition of strain A and B (blue and red marbles), each reaches a limit, but in general these limits differ from one another. Once all of the subpopulations in an ensemble reach their limit, the distribution of the population composition freezes to a steady state, which is equal to the probability distribution of x^* . Similar random limit properties appear in other fields, with *lock-in* in economics as the best-known example [30].

The inset in Fig 2 shows approximate solutions for the time evolution of mean, standard deviation, and skewness of the composition x , which we obtained by analytically solving the Master Eq (1) (see S2 Text). The analytical results agree well with their numerical counterparts. In particular, the mean value remains constant over time, as it must for a non-selective process.

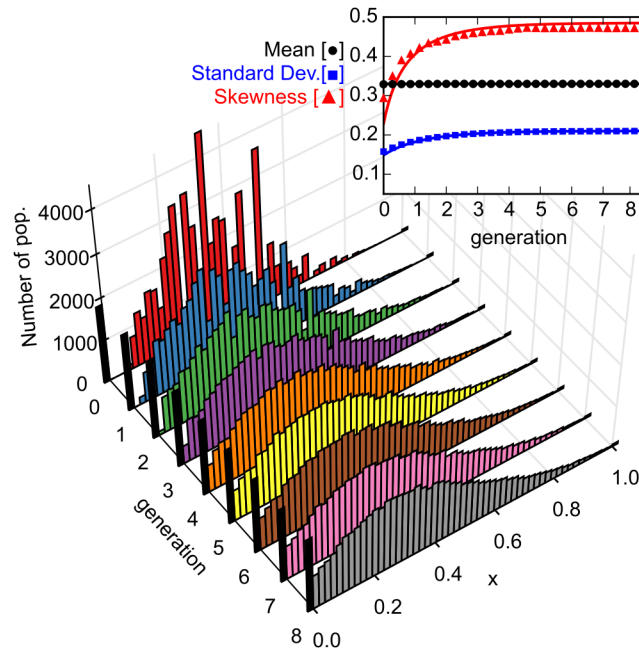


Fig 2. Time series for the simulated distribution of the population composition x . The distribution initially broadens, then freezes to a steady state (see [S1 Video](#)). The fraction of populations that have $x = 0$ or $x = 1$ (indicated by the black bins) remains constant during the time evolution, as expected for a Pólya urn process, and in contrast to expectations from genetic drift (see [S1 Table](#)). In each well the population follows a stochastic path and reaches a (random) limit composition, and the distribution freezes only when all populations reached their limit. The parameter values used in the simulation are $\bar{N}_0 = 10$ and $\bar{x}_0 = 0.33$. The inset shows the mean, standard deviation and skewness as a function of the number of generations, with symbols denoting numerical simulations, and the solid lines corresponding to the theoretical prediction of [Eq \(2\)](#) (and also those in [S2 Text](#)). Analytical and numerical values agree. The mean ($\langle x \rangle$) remains constant throughout the evolution, as expected for a non-selective process; standard deviation and skewness saturate to limit values, confirming the freezing of the distribution.

doi:10.1371/journal.pone.0134300.g002

For the time evolution of the variance, which is a measure for the spread of a distribution, we obtain to leading order in population size

$$\text{Var}_{\text{poi}}[x](t) = \frac{2 - e^{-t}}{\bar{N}_0} \bar{x}_0 (1 - \bar{x}_0). \quad (2)$$

The broadening and freezing of the distribution is reflected in the exponential decay term of the variance. Note that the skewness increases as well, because growth is self-reinforcing (see inset in [Fig 2](#)). To further test the validity of the stochastic simulations, we also calculated the limit values of the average and variance after extended periods of evolution exactly, and found that they match the numerical solutions of the Master Equation perfectly (see [S1 Text](#)).

We tested these theoretical predictions using *P. putida* as a bacterial model system. We mixed the wild-type and mutant strains in order to obtain different initial fractions \bar{x}_0 . The degree of dilution of the mixture determines the average initial cell number \bar{N}_0 , with which we inoculated 120 wells per experiment (96-well plate format). In order to compare the experimental data with our model, we set up simulations that matched the experimental configuration by initializing \bar{N}_0 and \bar{x}_0 with the same values as measured in the experiments. We simulated the time evolution of about 10^4 populations, grouped in “virtual plates” of 120 wells each. Every virtual plate produced a histogram like the one we obtained from experiments. We then generated an average histogram of the virtual plates and used its values to compute the

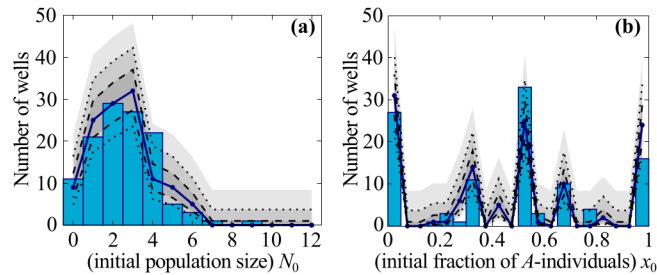


Fig 3. Initial distributions for population size N_0 and composition x_0 (parameter values $\bar{N}_0 = 2.55$, $\bar{x}_0 = 0.45$). The experimental distributions (bars) for N_0 (panel (a)) and x_0 (panel (b)) are measured from 120-well ensembles. The average \bar{N}_0 and \bar{x}_0 calculated from the measured values determine the parameters for the simulated distributions. The theoretical average distribution (solid blue line) is the average of the same distributions generated for 84 sets of 120 wells. Using that average we calculate the Wilson binomial confidence intervals (gray areas) for 68% (between dashed lines), 95% (between dotted lines) and 99.73% confidence. The measured and simulated distributions agree well within statistical error, confirming our assumption that individuals of strain A and B in the experiments start Poisson-distributed with mean $\bar{N}_0 \bar{x}_0$ and $\bar{N}_0(1 - \bar{x}_0)$, respectively. The ragged distribution of x_0 derives from a small-number effect, and disappears at larger values of N_0 (see main text, and also S3 Fig).

doi:10.1371/journal.pone.0134300.g003

binomial confidence intervals [36] for the count in each bin, and compared those with the experimental distribution.

Fig 3(a) shows a representative experimental histogram of the initial population sizes N_0 for strong dilution with $\bar{N}_0 = 2.55$. It is well approximated by a Poisson distribution, and agrees with the simulation results within statistical errors (blue line and shaded gray areas in Fig 3(a)). Fig 3(b) shows the probability distribution of the corresponding initial compositions x_0 of the populations, where again theoretical and experimental values agree well within statistical error. Note also that in every well the composition x_0 must be a simple fraction; this means that only a few numerical values are possible for small initial population sizes N_0 . This small-number effect explains why the distribution of x_0 in Fig 3(b) is so ragged. The distribution becomes much smoother for larger initial population sizes (see S3 Fig). Taken together, these results for the distribution of initial population size and composition confirm that the inoculation of the individual wells is a stochastic sampling process with Poissonian statistics.

Next, we were interested in how the composition of the bacterial population would evolve under non-selective (neutral) growth conditions. To this end we let the 120 populations grow for an 11-hour period, during which they remained in exponential growth phase (see S2 Fig). Then we measured the population size $N(t)$ in each well by counting colony-forming units, and $x(t)$ by counting the pyoverdine-producing colonies (see Materials and Methods). Fig 4 shows the final outcome for four different initial conditions, i.e. combinations of the initial average population size \bar{N}_0 and composition \bar{x}_0 . We first wanted to know what determines the number of wells that contain only individuals of either strain A or strain B, i.e. that are fixated. To this end we compared the experimentally observed values with the corresponding predictions from the numerical simulations of the Pólya urn model (Fig 4). Since both results agree within statistical error, we conclude that fixation of a population is a consequence of the initial sampling process and is not due to fixation during population growth (see also S1 Table). This is especially obvious for small average initial population size or compositions close to $x = 0$ or $x = 1$, where a large fraction of the wells contains cells of strain A or B only (Fig 4(a) and 4(d)). Next we wished to learn how the final distribution of the population composition (i.e. the random limits, x^*) depends on the initial average composition \bar{x}_0 . For $\bar{x}_0 = 0.5$, we observed both by experiment and theoretically that the initial distribution significantly broadened (by a factor

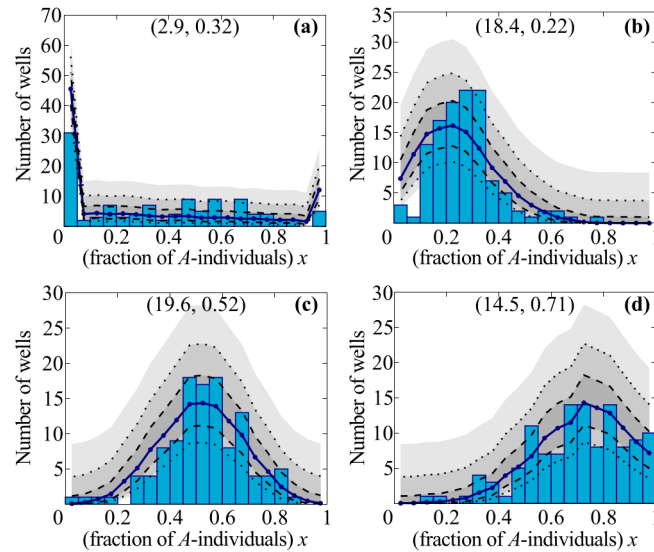


Fig 4. Steady-state distributions of population composition x for different initial conditions. The experimental distribution (bars) is the result of growth on 120 independent wells. We use the measured average \bar{x}_0 and N_0 from the experiments to initialize the simulations of several 120-well ensembles. After growth, we compute the histogram for each of these ensembles and obtain the average theoretical distribution (blue line). Using the values from this distribution, we compute the three confidence intervals (shaded gray areas) for each bin for 68% (between dashed lines), 95% (between dotted lines) and 99.73% confidence. The two sets of data match: most experimental data agree with the first prediction confidence region, practically all with the second one. The limit distributions are clearly different from the initial ones (see S1 Fig). The importance of growth in changing the distributions depends on the initial size N_0 (see main text, and S1 Fig). Parameter values: $N_0 = 2.9, \bar{x}_0 = 0.32$ (panel (a)); $N_0 = 18.4, \bar{x}_0 = 0.22$ (panel (b)); $N_0 = 19.6, \bar{x}_0 = 0.52$ (panel (c)); $N_0 = 14.5, \bar{x}_0 = 0.71$ (panel (d)).

doi:10.1371/journal.pone.0134300.g004

of $\sqrt{2}$) but remained symmetrical (Fig 4(c) and S1 Fig). In contrast, starting from distributions with average values below or above 0.5 caused the final distribution to broaden and also become skewed towards smaller or larger values of x , respectively (Fig 4(b) and 4(d)). Moreover, we found quantitative agreement between experiment and numerical simulations within statistical errors in all analyzed parameter regimes (see blue lines and shaded areas in Fig 4): most experimental histograms fall within the first confidence interval of the prediction (darkest gray areas, between dashed lines), and almost all fall within the 99.73% confidence interval.

Taken together, our combined theoretical and experimental analysis gives a coherent picture of evolution during non-selective (exponential) growth. We have shown, experimentally and by analogy with the Pólya urn model, that for each well-mixed population the composition of the population reaches a random stationary limit, and, unlike populations with constant size, generally does not fixate. For a large ensemble of populations, this implies that the probability distribution for the population composition converges to limit distributions (Figs 2 and 4), which are nothing like Kimura’s result for constant-sized populations. Our result is also quite different from that obtained in range expansion experiments [37] or other settings featuring population growth without death on two-dimensional substrates. There, monoclonal sectoring patterns arise as a consequence of random genetic drift, which drives population differentiation along the expanding fronts of bacterial colonies, unlike our well-mixed populations that freeze to coexistence.

Our study also shows that, in a growing population with stochastic initial conditions, demographic noise has two possible sources: the initial sampling process by which subpopulations are formed, and the subsequent growth process. The initial average population size \bar{N}_0 sets

their relative weight (see [S3 Text](#) and [S1 Fig](#)). For very small \bar{N}_0 , of the order of one or two individuals, the formation process already determines the final composition distribution: most populations start off fixated, many with just a single founder individual, and the composition of each well remains the same during growth. For very large \bar{N}_0 , of the order of a few hundreds, the sampling process is again central: the composition distribution changes very little before freezing, and growth generates only a very limited amount of variation. In these two limiting regimes, neglecting stochastic effects during growth leaves the evolutionary outcome practically unchanged. In contrast, for small founder colonies such as those typically found during population bottlenecks [[18](#), [19](#), [38](#)] ($\bar{N}_0 \sim 10$), population growth is responsible for the major part of the variation observed in the final distribution.

Moreover, our results reveal that a growing population reaches a random limit composition much faster than genetic drift leads to fixation in populations of constant size. Typical fixation times for genetic drift increase logarithmically with the population size [[11](#)], while the time scale for freezing is independent of population size. This has important consequences for the role of stochastic effects when a population passes from exponential growth phase to stationary phase, in which growth rate and death rate are equal. Then, the composition of the population shows both freezing and fixation, albeit at quite distinct times because the relevant time scales differ markedly. During growth the composition distribution quickly freezes, as described above. Once the population reaches its stationary size, it slowly drifts to fixation, following Kimura-like dynamics.

We also believe that our results have a broad range of applications since growing populations are ubiquitous in nature. For example, experimental studies of *P. aeruginosa* [[22](#), [39](#)] have shown that typical life cycles pass through different steps with regularly occurring dispersal events being followed by the formation of new colonies. As initial colony sizes are typically small, such dispersal events coincide with *population bottlenecks* and subsequent exponential growth. During these phases of the life cycle, population dynamics is often selectively neutral and hence falls within the framework of the present work. The degree of diversity generated during these population bottlenecks has been shown to be crucial for some proposed mechanisms for the evolution of cooperation under selective pressure [[5–7](#), [40–42](#)]. Our analysis quantifies the ensuing degree of diversity and points to the relative importance of sampling versus growth for long-term behavior of the reservoirs. This may have important consequences for the degree of genetic diversity observed in natural populations with life-cycle structures [[38](#)].

Materials and Methods

Strains and cultivation conditions

The *P. putida* strains KT2440 (wild type) and 3E2 (mutant with defective pyoverdine synthesis) [[3](#)] were used as pyoverdine producers and non-producers, respectively. Cells were grown in casamino acid medium (CAA) containing per liter: 5 g casamino acids, 0.8445 g K_2HPO_4 , 0.1404g $MgSO_4 \cdot (H_2O)$ [[3](#)]. The CAA medium was supplemented with 200 μM $FeCl_3$ (CAA-Fe) to suppress pyoverdine production (see [S2 Table](#)). Overnight cultures of the individual strains in CAA-Fe medium were adjusted to an OD_{600} of 1, diluted 10^{-2} fold, mixed to yield the desired producer fraction, and further diluted to create Poisson distribution conditions. Producer/non-producer co-cultures were started by inoculating the central 60 wells of two 96-well plates thereby adjusting the average initial cell number \bar{N}_0 to values between 2 and 25 cells/150 μL . Wells at the border of the plates were filled with water to minimize evaporation from central wells. For non-selective growth, co-cultures were grown in CAA-Fe medium shaking at 30°C for given periods of time. Due to the random distribution of initial cell number N_0 and producer fraction x_0 in the 120 wells, each experiment was unique. An experiment was

limited to 120 wells to allow initiation of the analysis of the subpopulations in the individual wells without uncontrolled changes of growth parameters during analysis. The experiment duration was set to 11h to allow evolution to act for a significant number of generations (see [S1 Table](#)), while leaving bacteria in exponential growth phase (see [S2 Fig](#))

Determination of growth parameters

Cell numbers N_0 and $N(t)$ were determined by counting the colony forming units (cfu) of individual wells. For this purpose 100 μ L aliquots of the individual wells were plated on cetrimide [43] or King's B agar (contains per liter: 20 g peptone, 10 g glycerol, 1.965 g $K_2HPO_4(3H_2O)$, 0.842 g $MgSO_4(H_2O)$ [44]. Producer fractions x_0 and $x(t)$ were determined based on the capability of cells to produce the green fluorescent pyoverdine either by direct counting of fluorescent and non-fluorescent colonies on the plates or after growth in iron-limited CAA medium. The fraction of dead cells was determined by life/dead staining with propidium iodide [45], and was always <0.02 of the total cell number under the experimental conditions.

Simulation of growing populations

We performed simulations of 10080 wells using a Gillespie algorithm [46]. The initial numbers of "cells" per well were drawn at random from a Poisson distribution with a mean value of \bar{N}_0 measured in the corresponding experiment. The strain assigned to every individual in each well was determined by the outcome of a Bernoulli trial (i.e., coin-flip-like process) and the probability of assignment to strain A was set to the value of \bar{x}_0 measured in the experiment. After initialization, wells were grouped into 84 virtual 120-well "plates", and a random waiting time was selected for each well, drawn from an exponential distribution with the population size as parameter. The Gillespie algorithm was run until the average size across all wells matched the average size measured at the end of the growth experiments, or until a specified time had elapsed (see [S2 Fig](#)).

Supporting Information

S1 Video. Time evolution of composition distribution. The distribution of compositions x first broadens due to demographic noise, but soon "freezes" to a steady state. The steady state form is maintained as long as the populations grow. Parameter values are $\bar{N}_0 = 10$, $\bar{x}_0 = 0.33$ (as for [Fig 2](#)).
(MP4)

S1 Text. Exact calculations for steady-state composition distribution and moments. Using the theory of Pólya urns, we calculate exactly the steady state values of: (i) the distribution of population compositions x , (ii) its mean value, and (iii) its variance.
(PDF)

S2 Text. Approximate calculations for the time evolution of the distribution moments. We use the Master equation of the growth process ([Eq \(1\)](#)) to determine the time evolution of variance and skewness of the composition distribution. These values are used in [Eq \(2\)](#) and [Fig 2](#).
(PDF)

S1 Fig. Initial and steady state distributions, relative entropy. Panels (a),(b),(c): Initial and final distributions of x for three regimes of \bar{N}_0 . When \bar{N}_0 is very small or very large (panels (a) and (b)), the evolutionary fate of the population is largely determined by the initial population sampling. Therefore, the initial distribution (red bars) and the steady-state one (green bars) look qualitatively very similar. For intermediate values of \bar{N}_0 , however, population growth

becomes more important, and the distributions look very different. The amount of composition values the population can access through growth can be quantified looking at the “unpredictability” of the steady-state composition, once the initial one is known: the more unpredictable, the more are made accessible by growth. Mathematically, the measure for this is called *conditional entropy*: the higher the entropy, the more unpredictable the outcome. Panel (d) shows the conditional entropy as function of \bar{N}_0 . Indeed, very small or very large initial populations experience little to no additional noise from growth, while in populations with intermediate values of \bar{N}_0 ($\bar{N}_0 \simeq 15$) growth is a major source of demographic noise. (Parameter values: $\bar{N}_0 = 2$ (a), $\bar{N}_0 = 2000$ (b), $\bar{N}_0 = 20$ (c); $\bar{x}_0 = 0.25$ in all panels) (TIF)

S3 Text. Comparison of initial and steady-state distributions of x , and entropy of the steady state distribution conditioned on the initial one. We use conditional entropy to analyze the impact of growth on the distribution of compositions x . The results are also depicted in [S1\(d\) Fig](#) (PDF)

S2 Fig. Growth curve of a mixed population. The population consists of pyoverdine producer (*P. putida* KT2440) and non-producer (*P. putida* 3E2) under non-selective (iron replete) conditions. Individual precultures of the strains were mixed and diluted in iron replete medium to yield $\bar{N}_0 = 4$ (in 150 μ L), and $\bar{x}_0 = 0.5$. Cells were grown aerobically at 30°C for 24 hours. The dots represent the mean $N(t)$ of three independent replications, the bars the corresponding standard deviation. After a lag phase of about 2 hours, the cells start to grow exponentially and reach the stationary phase after about 14 h of growth. For the non-selective growth experiments used to test the predictions of the Pólya urn model, cells were grown for 11.5 h to ensure exponential growth conditions. (TIF)

S3 Fig. Additional initial conditions measurements. The experimental distributions (bars) are measured from 120-well ensembles, the average N_0 and x_0 from those sets the parameters for the simulated distributions. The theoretical average distribution (solid line) is the average of the same distributions generated for 84 sets of 120 wells. Using that average we calculate three Wilson binomial confidence intervals (gray areas). Experiments and theory agree within statistical error: the distribution of sizes (panels (a) and (c)) follows a Poisson distribution. The raggedness of the distribution of x for at small \bar{N}_0 (see panel (b) and [Fig 3\(b\)](#) in main text) is due to a small size effect: since x must be a simple fraction, when N_0 is small only a few values are available (see main text). This effect disappears for average initial sizes $\bar{N}_0 \simeq 10$ (see panel (d)). Parameter values: $\bar{N}_0 = 5.75$, $\bar{x}_0 = 0.43$ (a) and (b); $\bar{N}_0 = 26.49$, $\bar{x}_0 = 0.45$ (c) and (d). (TIF)

S1 Table. Comparison between results from our experiments and those in [9]. While experiments for constant-sized populations of *Drosophila* observe significant fixations within the first tens of generations, we instead observe freezing of the probability distribution for the population composition, without any fixation. (PDF)

S2 Table. Comparison of growth and pyoverdine production per cell of *P. putida* KT2440 and 3E2. Separate cultures of producer (*P. putida* KT2440) and non-producer (*P. putida* 3E2) were grown in iron-limiting (no addition of FeCl_3) and iron-replete medium (addition of 200 μ M FeCl_3) at 30°C. The cell density was measured at 600 nm, and specific growth rates were calculated from density values of the exponential phase. The pyoverdine production was

determined by fluorescence emission measurements (excitation 400 nm, emission at 460 nm). The pyoverdine production per cell represents the ratio of pyoverdine fluorescence and optical density measured after 24 h of growth. The values in the table are averages over a minimum of five experiments, with the corresponding standard deviation. The fluorescence value for the non-producing mutant in iron-limiting medium is 0 because the culture failed to grow. (PDF)

Acknowledgments

For fruitful discussions we thank Madeleine Opitz, Johannes Knebel, Markus Weber, Stefano Duca, Matthias Bauer, Kirsten Jung. We thank Michelle Eder (HJ lab) for excellent technical assistance. *P. putida* strain 3E2 was kindly provided by P. Cornelis (Vrije Universiteit Brussels, Belgium).

Author Contributions

Conceived and designed the experiments: HJ FB. Performed the experiments: HJ FB. Analyzed the data: FB HJ ML KW EF. Contributed reagents/materials/analysis tools: EF ML KW. Wrote the paper: EF HJ ML KW. Designed theoretical analysis: EF ML KW. Performed theoretical analysis: ML KW.

References

1. Kimura M (1955) Solution of a process of random genetic drift with a continuous model. PNAS. PMID: [16589632](#)
2. Otto SP, Whitlock MC (1997) The probability of fixation in populations of changing size. Genetics 146: 723–733. PMID: [9178020](#)
3. Matthijs S, Laus G, Meyer JM, Abbaspour-Tehrani K, Schäfer M, et al. (2009) Siderophore-mediated iron acquisition in the entomopathogenic bacterium *pseudomonas entomophila* I48 and its close relative *pseudomonas putida* KT2440. Biometals 22: 951–964. doi: [10.1007/s10534-009-9247-y](#) PMID: [19459056](#)
4. Eggenberger F, Pólya G (1923) Über die statistik verketteter vorgänge. ZAMM—Journal of Applied Mathematics and Mechanics / Zeitschrift für Angewandte Mathematik und Mechanik 3: 279–289.
5. Melbinger A, Cremer J, Frey E (2010) Evolutionary game theory in growing populations. Phys Rev Lett 105: 178101. doi: [10.1103/PhysRevLett.105.178101](#) PMID: [21231082](#)
6. Cremer J, Melbinger A, Frey E (2011) Evolutionary and population dynamics: a coupled approach. Phys Rev E 84: 051921. doi: [10.1103/PhysRevE.84.051921](#)
7. Cremer J, Melbinger A, Frey E (2012) Growth dynamics and the evolution of cooperation in microbial populations. Sci Rep 2: 281. doi: [10.1038/srep00281](#) PMID: [22355791](#)
8. Crow JF, Kimura M (1970) An Introduction to Population Genetics. Harper and Row.
9. Hartl DL, Clark AG (1989) Principles of population genetics. Sinauer, Sunderland, MD, USA, 2nd edition.
10. Frey E, Kroy K (2005) Brownian motion: a paradigm of soft matter and biological physics. Ann Phys 14: 20–50. doi: [10.1002/andp.200410132](#)
11. Blythe RA, McKane J (2007) Stochastic models of evolution in genetics, ecology and linguistics. J Stat Mech: 07018. doi: [10.1088/1742-5468/2007/07/P07018](#)
12. Caballero A (1994) Developments in the prediction of effective population size. Heredity 73: 657–679. doi: [10.1038/hdy.1994.174](#) PMID: [7814264](#)
13. Gillespie JH (2001) Is the population size of a species relevant to its evolution? Evolution 55: 2161–2169. doi: [10.1554/0014-3820\(2001\)055%5B2161:ITPSOA%5D2.0.CO;2](#) PMID: [11794777](#)
14. Hahn MW (2008) Toward a selection theory of molecular evolution. Evolution 62: 255–265. doi: [10.1111/j.1558-5646.2007.00308.x](#) PMID: [18302709](#)
15. Hurst LD (2009) Fundamental concepts in genetics: genetics and the understanding of selection. Nat Rev Genet 10: 83–93. doi: [10.1038/nrg2506](#) PMID: [19119264](#)

16. Buri P (1956) Gene frequency in small populations of mutant drosophila. *Evolution* 10: 367–402. doi: [10.2307/2406998](https://doi.org/10.2307/2406998)
17. Center for Food Safety and Applied Nutrition Causes of Foodborne Illness: Bad Bug Book—BBB—*Escherichia coli* O157:H7 (EHEC). Provides basic information about *Escherichia coli* O157:H7.
18. Kurjak A, Chervenak FA (2006) *Textbook of Perinatal Medicine*. Informa UK Ltd, 2nd edition.
19. Grossart HP, Levold F, Allgaier M, Simon M, Brinkhoff T (2005) Marine diatom species harbour distinct bacterial communities. *Environmental Microbiology* 7: 860–873. doi: [10.1111/j.1462-2920.2005.00759.x](https://doi.org/10.1111/j.1462-2920.2005.00759.x) PMID: [15892705](https://pubmed.ncbi.nlm.nih.gov/15892705/)
20. Bird DF, Kalff J (1984) Empirical relationships between bacterial abundance and chlorophyll concentration in fresh and marine waters. *Can J Fish Aquat Sci* 41: 1015–1023. doi: [10.1139/f84-118](https://doi.org/10.1139/f84-118)
21. Buchan A, LeCleir GR, Gulvik CA, González JM (2014) Master recyclers: features and functions of bacteria associated with phytoplankton blooms. *Nat Rev Micro* 12: 686–698. doi: [10.1038/nrmicro3326](https://doi.org/10.1038/nrmicro3326)
22. Stoodley P, Sauer K, Davies DG, Costerton JW (2002) Biofilms as complex differentiated communities. *Annual Review of Microbiology* 56: 187–209. doi: [10.1146/annurev.micro.56.012302.160705](https://doi.org/10.1146/annurev.micro.56.012302.160705) PMID: [12142477](https://pubmed.ncbi.nlm.nih.gov/12142477/)
23. Levin SA (1974) Dispersion and population interactions. *The American Naturalist* 108: 207–228. doi: [10.1086/282900](https://doi.org/10.1086/282900)
24. Sanchez A, Gore J (2013) Feedback between population and evolutionary dynamics determines the fate of social microbial populations. *PLoS biology* 11: e1001547. doi: [10.1371/journal.pbio.1001547](https://doi.org/10.1371/journal.pbio.1001547) PMID: [23637571](https://pubmed.ncbi.nlm.nih.gov/23637571/)
25. Parsons TL, Quince C, Plotkin JB (2010) Some consequences of demographic stochasticity in population genetics. *Genetics* 185: 1345–1354. doi: [10.1534/genetics.110.115030](https://doi.org/10.1534/genetics.110.115030) PMID: [20457879](https://pubmed.ncbi.nlm.nih.gov/20457879/)
26. Buckling A, Harrison F, Vos M, Brockhurst MA, Gardner A, et al. (2007) Siderophore-mediated cooperation and virulence in *Pseudomonas aeruginosa*. *FEMS Microbiol Ecol* 62: 135–41. doi: [10.1111/j.1574-6941.2007.00388.x](https://doi.org/10.1111/j.1574-6941.2007.00388.x) PMID: [17919300](https://pubmed.ncbi.nlm.nih.gov/17919300/)
27. Cornelis P, Matthijs S, Van Oeffelen L (2009) Iron uptake regulation in *Pseudomonas aeruginosa*. *Bio-metals* 22: 15–22. doi: [10.1007/s10534-008-9193-0](https://doi.org/10.1007/s10534-008-9193-0) PMID: [19130263](https://pubmed.ncbi.nlm.nih.gov/19130263/)
28. Cohen JE (1976) Irreproducible results and the breeding of pigs (or nondegenerate limit random variables in biology). *BioScience* 26: 391–394.
29. Schreiber SJ (2001) Urn models, replicator processes, and random genetic drift. *SIAM Journal on Applied Mathematics* 61: 2148–2167. doi: [10.1137/S0036139999352857](https://doi.org/10.1137/S0036139999352857)
30. Sornette D (2009) *Why Stock Markets Crash: Critical Events in Complex Financial Systems*. Princeton University Press.
31. Pemantle R (2007) A survey of random processes with reinforcement. *Probability Surveys* 4: 1–79. doi: [10.1214/07-PS094](https://doi.org/10.1214/07-PS094)
32. Athreya KB, Karlin S (1968) Embedding of urn schemes into continuous time markov branching processes and related limit theorems. *The Annals of Mathematical Statistics* 39: 1801–1817. doi: [10.1214/aoms/1177698013](https://doi.org/10.1214/aoms/1177698013)
33. Kotz S, Mahmoud H, Robert P (2000) On generalized pólya urn models. *Statistics & Probability Letters* 49: 163–173.
34. Allen L (2003) *An Introduction to Stochastic Processes with Biology Applications*. Prentice Hall.
35. Arthur WB, Ermoliev YM, Kaniovski YM (1987) Path-dependent processes and the emergence of macro-structure. *European Journal of Operational Research* 30: 294–303. doi: [10.1016/0377-2217\(87\)90074-9](https://doi.org/10.1016/0377-2217(87)90074-9)
36. Wilson EB (1927) Probable inference, the law of succession, and statistical inference. *Journal of the American Statistical Association* 22: 209–212. doi: [10.1080/01621459.1927.10502953](https://doi.org/10.1080/01621459.1927.10502953)
37. Hallatschek O, Hersen P, Ramanathan S, Nelson DR (2007) Genetic drift at expanding frontiers promotes gene segregation. *PNAS* 104: 19926–19930. doi: [10.1073/pnas.0710150104](https://doi.org/10.1073/pnas.0710150104) PMID: [18056799](https://pubmed.ncbi.nlm.nih.gov/18056799/)
38. Hammerschmidt K, Rose CJ, Kerr B, Rainey PB (2014) Life cycles, fitness decoupling and the evolution of multicellularity. *Nature* 515: 75–79. doi: [10.1038/nature13884](https://doi.org/10.1038/nature13884) PMID: [25373677](https://pubmed.ncbi.nlm.nih.gov/25373677/)
39. Hall-Stoodley L, Costerton JW, Stoodley P (2004) Bacterial biofilms: from the natural environment to infectious diseases. *Nat Rev Microbiol* 2: 95–108. doi: [10.1038/nrmicro821](https://doi.org/10.1038/nrmicro821) PMID: [15040259](https://pubmed.ncbi.nlm.nih.gov/15040259/)
40. Chuang JS, Rivoire O, Leibler S (2009) Simpson's paradox in a synthetic microbial system. *Science* 323: 272–5. doi: [10.1126/science.1166739](https://doi.org/10.1126/science.1166739) PMID: [19131632](https://pubmed.ncbi.nlm.nih.gov/19131632/)
41. Oliveira NM, Niehus R, Foster KR (2014) Evolutionary limits to cooperation in microbial communities. *PNAS* 111: 17941–17946. doi: [10.1073/pnas.1412673111](https://doi.org/10.1073/pnas.1412673111) PMID: [25453102](https://pubmed.ncbi.nlm.nih.gov/25453102/)
42. Melbinger A, Cremer J, Frey E The emergence of cooperation from a single cooperative mutant.

43. Brown VI, Lowbury EJJ (1965) Use of an improved cetrinide agar medium and other culture methods for *pseudomonas aeruginosa*. *J Clin Pathol* 18: 752–756. doi: [10.1136/jcp.18.6.752](https://doi.org/10.1136/jcp.18.6.752) PMID: [4954265](https://pubmed.ncbi.nlm.nih.gov/4954265/)
44. King EO, Ward MK, Raney DE (1954) Two simple media for the demonstration of pyocyanin and fluorescin. *Journal of Laboratory and Clinical Medicine* 44: 301–307. PMID: [13184240](https://pubmed.ncbi.nlm.nih.gov/13184240/)
45. Suzuki T, Fujikura K, Higashiyama T, Takata K (1997) DNA staining for fluorescence and laser confocal microscopy. *J Histochem Cytochem* 45: 49–53. doi: [10.1177/002215549704500107](https://doi.org/10.1177/002215549704500107) PMID: [9010468](https://pubmed.ncbi.nlm.nih.gov/9010468/)
46. Gillespie D (1976) General method for numerically simulating stochastic time evolution of coupled chemical reactions. *J Comp Phys* 22: 403–434.